UNIVERSITY OF Nebraska Omaha

University of Nebraska at Omaha

DigitalCommons@UNO

Physics Faculty Publications

Department of Physics

5-2017

Kinematics of subluminous O and B stars by surface helium abundance

P. Martin

C. S. Jeffery

Naslim N.

V. M. Woolf

Dr. C.C. and Mabel L. CRISS LIBRARY

Kinematics of subluminous O and B stars by surface helium abundance

P. Martin,[1,2]★ C. S. Jeffery,[1,2] Naslim N.[1,3] and V. M. Woolf[4]

[1]*Armagh Observatory and Planetarium, College Hill, Armagh BT61 9DG, UK*
[2]*School of Physics, Trinity College Dublin, College Green, Dublin 2, Ireland*
[3]*Academia Sinica Institute of Astronomy and Astrophysics, Taipei 10617, Taiwan, Republic of China*
[4]*Department of Physics, University of Nebraska at Omaha, 6001 Dodge Street, Omaha, NE 68182, USA*

ABSTRACT

The majority of hot subdwarf stars are low-mass core-helium-burning stars. Their atmospheres are generally helium deficient; however, a minority have extremely helium-rich surfaces. An additional fraction have an intermediate surface-helium abundance, occasionally accompanied by peculiar abundances of other elements. We have identified a sample of 88 hot subdwarfs including 38 helium-deficient, 27 intermediate-helium and 23 extreme-helium stars for which radial-velocity and proper-motion measurements, together with distances, allow a calculation of galactic space velocities. We have investigated the kinematics of these three groups to determine whether they belong to similar or different Galactic populations. The majority of helium-deficient subdwarfs in our sample show a kinematic distribution similar to that of thick disc stars. Helium-rich sdBs show a more diverse kinematic distribution. Although the majority are probably disc stars, a minority show a much higher velocity dispersion consistent with membership of a Galactic halo population. Several of the halo subdwarfs are members of the class of 'heavy-metal' subdwarfs discovered by Naslim et al.

Key words: stars: chemically peculiar – stars: kinematics and dynamics – subdwarfs.

1 INTRODUCTION

Hot subluminous stars or subdwarfs are traditionally classified into three types by their spectra (Drilling et al. 2003). Subdwarf B (sdB) stars have a surface effective temperature T_{eff} in the range 20 000–40 000 K and hydrogen-Balmer absorption lines wider than in normal B stars; subdwarf O (sdO) stars, with T_{eff} ranging from 40 000–80 000 K have strong He^+ absorption lines; subdwarf OB (sdOB) stars represent a transition between O and B types (Moehler et al. 1990; Heber 2009). These objects are located below the upper main sequence on a Hertzsprung–Russell diagram. Identified as low-mass core-helium burning stars with low-mass envelopes, they are also known as extreme horizontal branch (EHB) stars.

The atmospheres of sdB stars are generally helium deficient, as radiative levitation and gravitational settling cause helium to sink below the hydrogen-rich surface (Heber 1986), deplete other light elements and enhance many heavy elements in the photosphere (O'Toole & Heber 2006). However almost 10 per cent of the total subdwarf population comprises stars with helium-rich atmospheres. The helium-rich subdwarfs may be further divided into extremely helium-rich stars and a small number of intermediate helium-rich stars, a number of which show extreme chemical peculiarities (Naslim et al. 2011, 2013). A recent review of hot subluminous stars has been given by Heber (2016).

The formation of hot subdwarfs offers several puzzles; they are observed as single stars and as both close and wide binaries. The helium-deficient sdOs are likely the progeny of sdB stars in a post-EHB phase as they have diffusion-dominated abundance patterns and similar binary frequencies (Heber 2009). Binary interaction via one or two common-envelope ejection phases provides a very promising mechanism to explain the many close binaries found amongst the sdB stars (Han et al. 2002, 2003). Extreme-helium subdwarfs appear to be well explained by the merger of two helium white dwarfs (Zhang & Jeffery 2012). However, it is harder to understand the intermediate-helium subdwarfs; few have been analysed and those that have are diverse (Naslim et al. 2011, 2012, 2013).

As the atmospheric abundance patterns of hot subdwarfs are governed by diffusion processes, they cannot be used to establish population membership. However, stars in the Milky Way formed at different epochs belong to different populations, which can be distinguished via kinematic criteria. Kinematical data give us access to the motions of the different populations of stars in the Galaxy. Some components of the Milky Way are rapidly rotating with little dispersion in the velocities of the members while others show only little rotation but high dispersions. Orbital eccentricity may also distinguish between younger and older stars as more gravitational

★ E-mail: pam@arm.ac.uk

interactions lead to larger deviations from originally circular orbits (if that is where the progenitors formed).

Members of the thin disc population are found close to the Galactic plane in low eccentricity orbits. Heliocentric velocities of thin disc stars in the solar neighbourhood are small. Stars of the thick disc population orbit around the Galactic Centre on more eccentric orbits and are found at higher distances from the plane. Typically, velocities are larger, relative to the local standard of rest (LSR), than for thin disc objects. Stars of the Galactic halo population (also known as Population II stars) are often found at large distances from the galactic disc and their orbits are often highly eccentric. Halo stars as a population do not (or not much) participate in the galactic rotation. These stars include those with the highest heliocentric velocities.

Previous studies involving the kinematics of sdBs found that the majority are members of the disc but that a minority are halo members (Altmann, Edelmann & de Boer 2004). Randall et al. (2015) have recently shown that the intermediate-helium sdB star LS IV−14°116 has halo kinematics. This raises the question of whether the helium-rich hot subdwarfs all belong to this halo minority and the 'normal' sdO/Bs are a disc population. In this paper, we collate radial velocities and proper motions for a significant sample of helium-deficient, intermediate-helium and extreme-helium subdwarfs, including a number of new measurements (Section 2). From these, we compute space velocities (Section 3) and galactic orbits in order to identify the parent populations (Section 4). We discuss some of the implications of these results for interpreting the origin of, in particular, the chemically peculiar intermediate-helium sdBs (Section 5).

2 DATA

We analysed a sample of 88 hot subdwarfs (sdO/B) including 38 helium-deficient, 27 intermediate-helium and 23 extreme-helium stars. The criterion for inclusion was that each star should have measurements of radial velocity, helium abundance, and proper motion; these are shown in Tables A1–A3.

2.1 *Radial velocities*

Radial velocities for 63 stars were obtained from the literature, as described in Tables A1–A3. A small number of these have errors in excess of 30 km s^{-1}; although large, the data were retained so as not to over-restrict the sample. The errors were propagated through the space motion calculations.

Radial velocities for 32 helium-rich hot subdwarfs were measured by us and are presented here (Table 1). Two spectra for 10 of these stars were obtained using the Ultraviolet and Visual Echelle Spectrograph (UVES) instrument on the ESO VLT, as part of the ESO supernova progenitor survey between 2000 and 2003 (Napiwotzki et al. 2003). Pipeline-reduced spectra were recovered from the ESO archive. Velocity shifts were measured by cross-correlation with an appropriately chosen model spectrum. Radial velocities for four stars observed in 2005 with the University College London Echelle Spectrograph (UCLES) on the Anglo–Australian Telescope were measured by cross-correlation with theoretical spectra corresponding approximately to the solutions obtained by Naslim et al. (2010). The dates and heliocentric radial velocities measured for each observation are shown in Table 1 with a mean uncertainty of ±4.6 km s^{-1}. The mean velocity for each star is represented as γ, and the error represents half the difference between the two measurements. For HE 0111−1526 and HE 1258+0113, these differences are, respectively, more than 8 and 5 times the mean differences of the remainder, suggesting that

one or both may be binaries. These stars have not been used in the kinematical analysis as the system velocity is unknown.

Five helium-rich sdO/B stars were observed with the High Dispersion Spectrograph (HDS) instrument on the *Subaru* telescope, operating in service mode on 2015 June 3. The data were reduced using standard IRAF procedures, the echelle orders were merged and wavelengths corrected for earth motion. Radial velocities of each star were measured by cross-correlation against a standard template. Two templates were used, being theoretical spectra for intermediate helium-rich hot subdwarfs and having effective temperatures of 34 000 and 40 000 K, the first being carbon-rich, the second nitrogen-rich. Two spectral windows were used with each template, covering a part of both CCDs in the HDS instrument, and hence giving four independent measurements of velocity for each observation. The means and standard deviations are given in Table 1. The radial velocities for the other 12 stars reported in Table 1 were measured from the blue part of the spectrum (4165–4570 Å) published by Ahmad & Jeffery (2003), using cross-correlation as for the *Subaru* data. The template was an extremely helium-rich model with effective temperature 40 000 K and surface gravity log g = 5.4.

Since binary companions affect the radial velocity of a star periodically, the system velocities, γ, were used for confirmed binary systems. We cannot exclude the possibility of unconfirmed binary systems that would affect the calculated Galactic velocities and orbits. Estimates of the binary fraction for EHB stars are between 50 and 60 per cent (Maxted et al. 2001; Copperwheat et al. 2011). This is a lower bound since the radial velocity variations of very long period systems are difficult to detect. All stars with single-epoch radial velocity measurements and confirmed binary systems are flagged in Tables A4– A6. These flagged stars should be considered as candidates for the thin disc, thick disc or halo populations until the radial velocities are confirmed.

2.2 *Abundances*

Subdwarf O and B stars can be further classified by their surface helium content. Based on the overall classification for hot subdwarfs developed by Drilling et al. (2013), extreme helium-rich subdwarfs are defined to have $n_{He} > 80$ per cent by number, intermediate helium-rich subdwarfs have a helium abundance of 5 per cent $< n_{He} < 80$ per cent and helium-deficient subdwarfs have $n_{He} < 5$ per cent. Helium abundances for the current sample were obtained from Ahmad et al. (2007); Edelmann (2003); Drilling et al. (2013); Geier et al. (2015); Naslim et al. (2010, 2013) and Stroeer et al. (2007), and the sample subdivided according to the above criteria.

Six intermediate-helium sdBs have been found to have unusual and interesting surface chemistries.

Edelmann (2003) found PG 0909+276 and UVO 0512−08 to show surface helium abundances of roughly 20 per cent by number, and extreme (3–4 dex) overabundances of scandium, titanium, vanadium, manganese and nickel.

LS IV−14°116 has a gravity slightly lower than that of normal sdB stars (log g = 5.6) and a surface helium abundance of about 16 per cent by number. It is slightly metal poor (−0.8 dex) relative to the Sun. What makes LS IV−14°116 distinct from any other hot subdwarf, whether helium rich or not, is the overabundance by 4 orders of magnitude of zirconium, yttrium and strontium and a 3 dex overabundance of germanium in the line-forming region of the photosphere (Naslim et al. 2011).

Two stars, HE 2359−2844 and HE 1256−2738, show optical absorption lines due to triply ionized lead (Pb IV) that have never previously been detected in any star (Naslim et al. 2013). The

Table 1. Heliocentric radial velocities for 32 helium-rich hot subdwarfs.

Star	Instrument	Date	RV (km s^{-1})	γ	$\pm$
HE 0001–2443	UVES	15/10/02	4.68	3.98	0.71
		18/06/03	3.27		
HE 0111–1526	UVES	18/12/01	6.56	−21.83	28.39
		29/12/01	−50.22		
HE 1135–1134	UVES	28/06/01	22.22	24.67	2.45
		24/07/01	27.11		
HE 1136–2504	UVES	22/04/00	68.6	59.39	9.22
		17/05/00	50.17		
HE 1238–1745	UVES	23/06/01	−10.58	−7.87	2.72
		23/07/01	−5.15		
HE 1256–2738	UVES	22/04/00	146.26	140.46	5.8
		19/05/00	134.66		
HE 1258+0113	UVES	19/05/00	−62.29	−42.69	19.6
		22/05/00	−23.09		
HE 1310–2733	UVES	22/04/00	39.72	41.54	1.82
		24/04/00	43.36		
HE 2218–2026	UVES	24/09/02	−278.91	−278.86	1.45
		25/09/02	−281.81		
HE 2359–2844	UVES	15/09/02	−93.74	−90.71	3.03
		25/09/02	−87.68		
UVO 0825+15	HDS	03/06/15	56.4		0.5
J092440.11+305013.16	HDS	03/06/15	2.7		0.5
J160131.30+044027.00	HDS	03/06/15	−27.4		0.9
J175137.44+371952.37	HDS	03/06/15	−73.6		0.2
J175548.50+501210.77	HDS	03/06/15	−62.7		0.2
PG 2321+214	HDS	04/10/98	−19.7		3
PG 0902+057	UES	06/05/95	−15		5
PG 1615+413	ISIS	31/05/96	−80		5
PG 1600+171	ISIS	31/05/96	−78		5
PG 1658+273	ISIS	31/05/96	−33		5
PG 1715+273	ISIS	31/05/96	31		5
HS 1844+637	ISIS	31/05/96	20		10
PG 1554+408	ISIS	31/05/96	73		8
PG 2258+155	ISIS	04/10/98	34		5
PG 1127+019	IDS	28/04/02	19		2
PG 1415+492	IDS	29/04/02	54		1
PG 2215+151	ISIS	31/05/96	−13		5
HS 1000+471	ISIS	31/05/96	0		10
BPS CS 22956–0094	UCLES	27/08/05	−4.1		1
BPS CS 29496–0010	UCLES	27/08/05	−39.8		0.1
BPS CS 22940–0009	UCLES	26/08/05	47.8		0.5
LB 3229	UCLES	27/08/05	42.7		1.0

atmospheric abundance of lead is nearly 10 000 times that measured in the Sun. HE 2359–2844 also shows zirconium and yttrium abundances similar to those in the zirconium star LS IV−14°116. UVO 0825+15 has just been discovered to be a variable lead-rich hot subdwarf (Jeffery et al. 2017).

2.3 *Proper motions*

The proper motions used in this work were taken from either the PPMXL or the NOMAD catalogues (Zacharias et al. 2004; Roeser, Demleitner & Schilbach 2010), adopting the value with the smaller error wherever more than one value was available. Proper motions were obtained from *Gaia* DR1 (Gaia Collaboration 2016a,b; Lindegren et al. 2016; Arenou et al. 2017) for JL 87 and SB 705. The mean error of the proper motions is ±3.91 mas yr^{-1}. Large catalogues such as PPMXL and NOMAD inevitably contain errors and extreme values due to outliers. For this reason, the proper motions obtained for this paper were compared with the UCAC4 catalogues;

all proper motions agree within errors where the catalogues overlap. A study of the problems of outliers is discussed in Ziegerer et al. (2015).

2.4 *Distances and reddening*

Distances were estimated from photometry using the distance modulus

$$\mu = 5 \log_{10} d - 5 + A_{\rm B}, \tag{1}$$

where $\mu = m_{\rm B} - M_{\rm B}$ and $A_{\rm B} = 4.1 E_{\rm B\text{-}V}$. $M_{\rm B}$ is the absolute magnitude and $m_{\rm B}$ is the apparent magnitude in B. Values for $m_{\rm B}$ were taken from SIMBAD and those for $M_{\rm B}$ were taken from the literature (references in Tables A1–A3). Only 45 per cent of stars in this sample had published values for $M_{\rm B}$, for the remainder estimates were made by assuming the means of these values, which are 4.14 mag for the helium-rich and 3.99 mag for the helium-deficient sdO/Bs. The reddening values ($A_{\rm B}$) were found using a dust extinction tool, hosted by the NASA/ IPAC Infrared Science

Table 2. Calculated distances in kpc compared with published values.

Star	Calculated distance	Published distance
HE 0004−2737	0.62 ± 0.09	0.67^{a}
HE 0151−3919	1.07 ± 0.27	0.92^{a}
HS 0232+3155	1.95 ± 0.27	1.70^{a}
HS 0233+3037	1.23 ± 0.17	1.00^{a}
HE 0407−1956	0.86 ± 0.12	0.89^{a}
HS 0546+8009	1.10 ± 0.15	1.00^{a}
HS 0815+4243	2.60 ± 0.35	2.50^{a}
PG 1136−003	0.87 ± 0.23	1.3 ± 0.2^{b}
HS 1236+4754	1.99 ± 0.27	2.10^{a}
HS 1320+2622	3.14 ± 0.43	3.40^{a}
HS 1739+5244	1.76 ± 0.24	1.80^{a}
HS 1741+2133	1.95 ± 0.27	1.80^{a}
HE 2135−3749	0.66 ± 0.10	0.71^{a}
HS 2156+2215	3.05 ± 0.42	2.80^{a}
HS 2201+2610	0.95 ± 0.13	0.90^{a}
HS 2208+2718	1.28 ± 0.18	1.20^{a}
HS 2242+3206	1.48 ± 0.20	1.30^{a}
HE 2337−2944	0.90 ± 0.13	0.96^{a}
CD−35°15910	0.22 ± 0.06	0.22 ± 0.08^{c}
PG 2352+181	0.38 ± 0.06	0.90 ± 0.32^{d}

Notes. [a]Edelmann (2003), [b]Geier et al. (2015), [c]van Leeuwen (2007), [d]Colin et al. (1994)

Figure 1. Histogram of the Galactic rotational velocities of all 88 stars of the sample.

Archive, which gives the Galactic dust reddening for a line of sight, returning a reddening map that is a reprocessed composite of the COBE/DIRBE and *IRAS*/ISSA maps (Schlafly & Finkbeiner 2011). The large reddening corrections to the KPD stars may be overestimated by this method due to their low Galactic latitudes. Hence, their distances are likely underestimated.

Distances, from a variety of methods, were found in the literature. These were compared with the calculations performed here (Table 2). Out of the 20 distances compared, there was a 95 per cent agreement. Distances for JL 87 and SB 705 were taken from the Astraatmadja & Bailer-Jones (2016) catalogue that make use of the *Gaia* DR1 parallaxes.
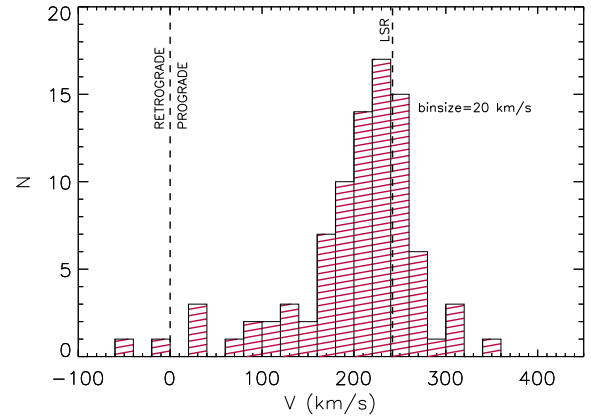
3 KINEMATICS

3.1 Calculating galactic velocities

Using the observed values of right ascension, declination, distance, proper motion and radial velocity, the Galactic velocity components were calculated following the method outlined in Randall et al. (2015). The left-handed system for the velocity components is used here, where U is the Galactic radial velocity, positive towards the Galactic Centre, V is the Galactic rotational velocity in the direction of the Galactic rotation and W is the component positive towards the North Galactic Pole. This calculation assumes the distance of the Sun from the Galactic Centre to be 8.4 kpc, its motion relative to the LSR to have components $(v_x, v_y, v_z) = (11.1, 12.24, 7.25)$ km s^{-1} and the velocity of the LSR to be $V_{LSR} = 242$ km s^{-1} (Irrgang et al. 2013).

3.2 Galactic velocities and velocity dispersions

Fig. 1 shows the distribution of rotational velocity, V, for all 88 stars. A peak can be seen at 220 km s^{-1}, near the LSR where disc stars are expected to be. This has also been found by Pauli et al. (2006) for their white dwarf sample. This distribution is similar to the sample of 114 sdBs analysed by Altmann et al. (2004), who also found a similar peak and a tail of the distribution extending into negative rotational velocities.

The kinematics of this sample were first investigated using a $U - V$ velocity diagram. In Fig. 2, the Galactic radial velocity U is plotted versus the Galactic rotational velocity V. The dotted ellipses correspond to the 3σ-thick and 3σ-thin disc distributions of white dwarfs as calculated by Pauli et al. (2006), who classified a sample of 398 white dwarfs based on their position in the $U - V$ diagram, the position in the J_z – eccentricity diagram and the stars Galactic orbit combined with age information. In the $U - V$ diagram (Fig. 2), the helium-deficient stars (green) are mostly clustered around the LSR (black star). The helium-rich stars (intermediate and extreme) are more widely distributed in this plot. Two of these stars have possible retrograde orbits, with their Galactic rotational velocities being negative, they are labelled in Fig. 2. HE 2218−2026 lies far outside the disc distributions with a high Galactic radial velocity of almost 300 km s^{-1}.

Another method of analysing the kinematics of stars is to look at their total velocity or kinetic energy. In Fig. 3, the kinetic energy $2E_{kin}/m = U^2 + V^2 + W^2$ is plotted against the rotational velocity V. Included in this graph are contours showing the velocities perpendicular to Galactic rotation at certain values, where $v_\perp = (U^2 + W^2)^{1/2}$. The higher the value of $2E/m$ the more an object deviates from a circular orbit. For low values of $v_\perp$, the deviation from LSR gives information about the kinetic temperature. The clustering of values around $v_\perp = 0$ means that they are kinematically cool. A few stars are located further away from the $v_\perp = 0$ contour; these are the kinematically hot stars and likely to have a more eccentric orbit. Another reason for a large proportion of stars with low $v_\perp$ could be that they are near their orbital turning point. Table 3 shows the mean values and standard deviations of the galactic velocities for the hot subdwarf helium classes as compared with previous studies. The Galactic velocities and corresponding errors for individual stars are shown in appendix Tables A4–A6.

4 GALACTIC ORBITS

4.1 Calculating the orbits

In addition to Galactic velocities, the orbits were calculated for the stars in this sample. This was achieved using galpy, a PYTHON package for Galactic-dynamic calculations (Bovy 2015). The orbits
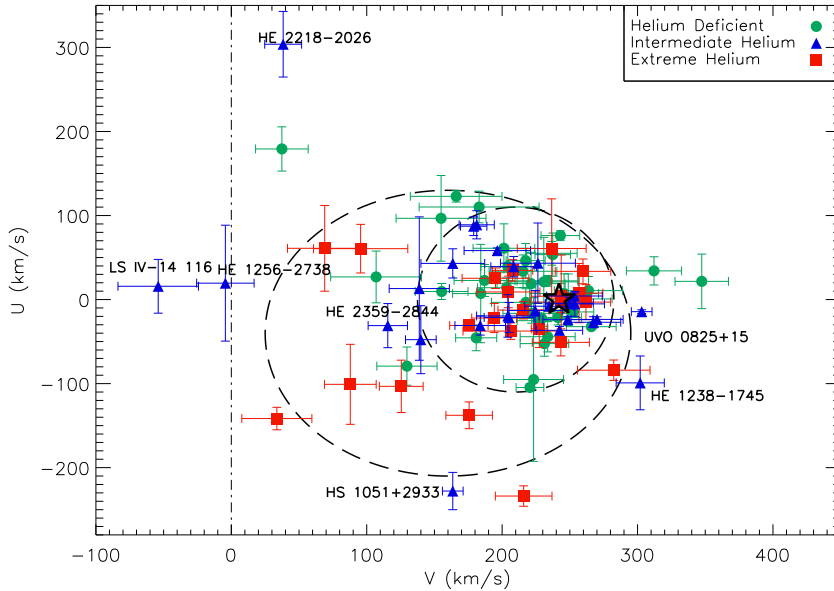
Figure 2. $U - V$- velocity diagram with 3σ (thin disc) and 3σ (thick disc) contours. Red squares are extremely helium-rich subdwarfs, blue triangles are intermediate helium-rich subdwarfs and the green data circles are the helium-deficient stars. The black star represents the local standard of rest (LSR). The dot–dashed line at a Galactic rotational velocity of zero is to highlight stars with retrograde motion.
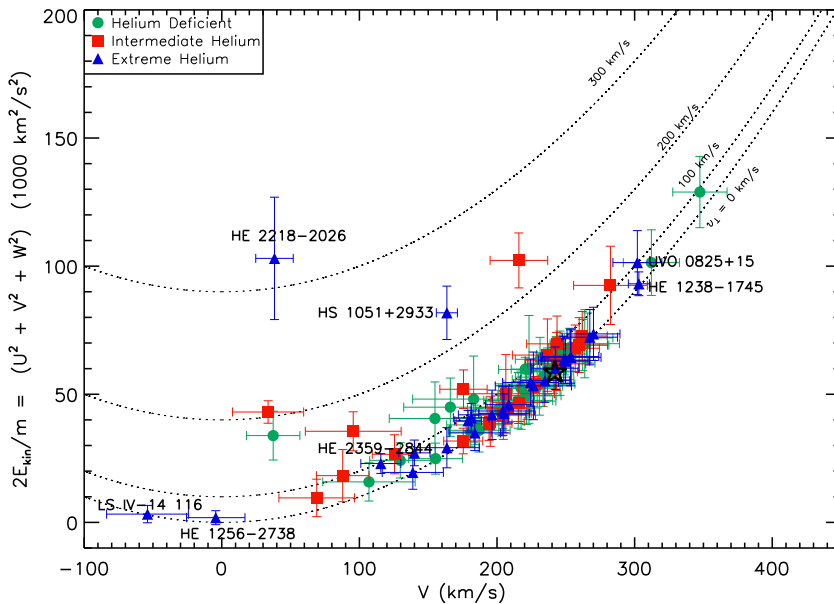

Figure 3. Galactic rotational velocity against the total kinetic energy. Symbols have the same meaning as above. The parabolic curves denote line of equal velocity $v_\perp = (U^2 + W^2)^{1/2}$.

were computed using the potential MWPotential 2014; this model is fit to dynamical data of the Milky Way. Although this is not the best possible current model, it was chosen as it gives a realistic model of the Milky Way's gravitational potential that is simple and easy to use. It consists of a bulge modelled as a power-law density profile that is exponentially cutoff with a power-law exponent of −1.8 and a cut-off radius of 1.9 kpc, a Miyamoto–Nagai Potential disc (Miyamoto & Nagai 1975) and a dark-matter halo described by a Navarro–Frenk–White potential (Navarro, Frenk & White 1996). The distance of the Sun from the Galactic Centre is set to 8.4 kpc and the velocity of the LSR is $V_{LSR} = 242$ km s^{-1}.

Extracted from these orbits, integrated over ≈ 3G yr, are the quantities apocentre, R_a, pericentre, R_p, eccentricity, e, maximum vertical amplitude, z_{max} and normalized z-extent, z_n. The quantities R_a and R_p are the maximum and minimum distances from the Galactic Centre attained during a revolution of 2π radians, measured on the Galactic plane. From these distances we find the eccentricity that is given by

$$e = \frac{R_a - R_p}{R_a + R_p}. \tag{2}$$

Table 3. Mean values and standard deviations of the hot subdwarf helium classes. Results from Altmann et al. (2004) and Pauli et al. (2006) are also shown here.

Subsample	N	$\overline{U}$	σ_U	$\overline{V}$	σ_V	$\overline{W}$	σ_W
All	88	−1.7	72.6	202.2	67.6	5.6	49.0
Helium-deficient	38	14.1	56.7	215.0	52.9	−4.4	39.8
Intermediate-helium	27	3.1	83.3	190.2	84.7	13.4	35.5
Extreme-helium	23	−30.4	72.6	193.8	65.9	13.9	69.9
Altmann	114	−8	74	198	79	12	64
Pauli WD thin disc	361	...	34	...	24	...	18
Pauli WD thick disc	27	...	79	...	36	...	46
LSR	...	0	...	242	...	0	...

Figure 5. Histograms of the eccentricity distribution. Top left: intermediate-helium, top right: extreme-helium, bottom left: helium-deficient, bottom right: all.

4.2 The orbits and orbit parameters

Fig. 5 shows histograms of the eccentricity distribution of the three helium classes. The He-deficient and total group of stars has a peak of $e \approx 0.2$; this region is mainly populated by disc stars. The He-enriched stars, on the other hand, have a distribution widely spread over the whole range.

Our classification scheme has been adopted from Pauli et al. (2003, 2006). Ma et al. (2016) found a vertical scale height for the thick disc between 1 and 1.5 kpc, so here we have set 1.5 kpc as the cut-off height for the thin disc.

(i) Stars whose orbits have low eccentricity and low inclination on the Galactic plane are referred to as the thin disc component. These stars must lie within Region 1 in the $J_z - e$ diagram and within the 3σ-thin disc contour and have $z_{max} < 1.5$ kpc.

(ii) Stars that lie in Region 2 and the 3σ-thick disc contour have been classified as belonging to the thick disc.

(iii) Stars that have been classified as halo lie outside Regions 1 and 2 and lie outside both 3σ contours and have a $z_{max} > 1.5$ kpc. All orbits have also been visually inspected as part of the classification.

Table 5 shows the number of stars classified as halo, thin or thick disc stars. The thin and thick discs kinematically overlap one another in a way that makes it difficult to find selection criteria capable of distinguishing them from one another. It has been suggested by Bovy (2011) that there is actually no thin/thick disc dichotomy and that the transition between thin and thick discs is rather a continuum of discs.

There is a large variety of orbit morphologies in this sample. Fig. 6 shows the meridional sections of the orbits of 18 stars. Row 1 contains intermediate-helium stars, row 2 contains extreme-helium sdO/Bs and row 3 shows the orbits of the helium-deficient sdO/Bs.
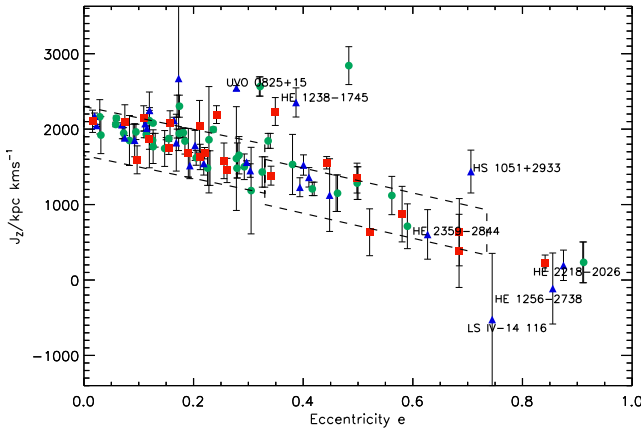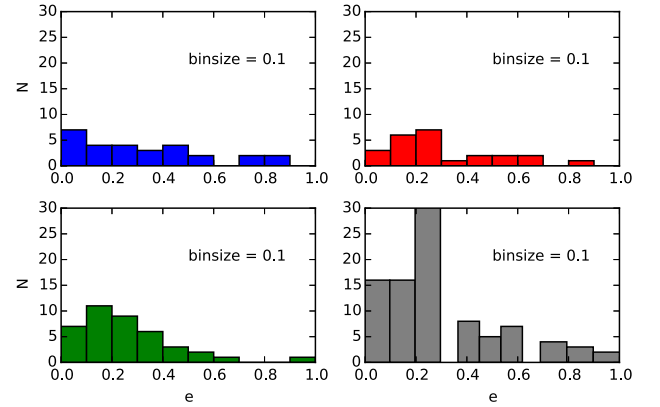

Figure 4. Z-component of the angular momentum versus eccentricity. Symbols have same meaning as previous plots. Eccentricity errors have been removed for clarity.

The normalized z-extent of the orbit, which can be used as a measure for the inclination of an orbit, is given by

$$z_n = \frac{z_{max}}{R(z_{max})} \tag{3}$$

where R is the galactocentric distance. These quantities are shown in Tables A4–A6, along with the star's Galactic velocities. The mean values and standard deviations for the parameters e, z_n and z_{max} are shown in Table 4.

Two important orbital parameters are the z-component of the angular momentum J_z and the eccentricity of the orbit. Fig. 4 shows a plot of J_z versus eccentricity. This diagram can be used to distinguish different populations. The thin disc stars cluster in an area of low eccentricity and J_z around 1800 kpc km s^{-1}. Pauli et al. (2003) call this Region 1. The thick disc stars possess higher eccentricities and lower angular momenta called Region 2. Those stars that lie outside these regions are halo candidate stars.

Table 4. Mean values and standard deviations of the orbital parameters eccentricity, maximum z-extent, maximum vertical amplitude, apocentre and pericentre, respectively.

Subsample	N	$\overline{e}$	σ_e	$\overline{z_n}$	σ_{z_n}	$\overline{z_{max}}$	$\sigma_{z_{max}}$	$\overline{R_a}$	σ_{R_a}	$\overline{R_p}$	σ_{R_p}
All	88	0.29	0.22	0.23	0.35	1.76	2.55	10.03	2.85	5.70	2.26
Helium-deficient	38	0.26	0.18	0.16	0.17	1.19	1.18	9.91	2.75	5.99	1.97
Intermediate-helium	27	0.32	0.23	0.27	0.41	1.92	3.02	10.31	2.78	5.49	2.39
Extreme-helium	23	0.32	0.23	0.31	0.34	2.53	2.78	9.91	2.57	5.44	2.44

Table 5. Population classification.

Subsample	N	Thin disc	Thick disc	Halo
All	88	45	36	7
Helium-deficient	38	25	12	1[a]
Intermediate-helium	27	13	10	4
Extreme-helium	23	7	14	2

Notes. [a] The halo classification for the helium-deficient HS 2208+2718 should be considered provisional, as there is a non-zero probability, that is, it is a radial velocity variable.

Columns 1–3 are examples of disc stars and columns 4–6 show halo orbits. The same layout applies to Fig. 7 that shows the orbits projected on to the *x–y* Galactic plane.

5 DISCUSSION

In general, hot subdwarfs show a much larger distribution in velocity than white dwarfs. Fig. 2 shows that the helium-deficient subdwarfs are more clustered around the LSR that suggests that they are likely disc stars with some having possible thin disc kinematics. Two of the chemically peculiar sdBs have a very low or even retrograde rotational velocity indicating that they have halo kinematics. The kinetic energy diagram (Fig. 3) shows that a significant portion of the sample has kinematics that are solar-like, suggesting membership of the thin disc. The mean values and standard deviations of the galactic velocities of the entire sample of sdO/Bs agree amiably with Altmann's study of 114 sdBs. Examining the helium-deficient velocity distribution alone (Table 3), it may be seen that the classical sdB stars fit closer to Pauli's white-dwarf thick-disc sample than to Altmann's sample. The helium-rich groups have much higher standard deviations (Table 3), suggesting that there is more of a halo contribution to these subgroups. Kawka et al. (2015) calculated the Galactic velocity components of all known hot subdwarf binary systems. They found that the population kinematics imply an old

age and include a few likely halo population members and that the hot subdwarf binary population has a velocity dispersion between the thin and thick disc dispersions for white dwarfs.

Special attention has been paid to intermediate-helium stars with peculiar surface chemistries (Figs 6 and 7).

LS IV–14°116 (Zr, Y, Sr, Ge) initially appears to have a disc orbit due to its maximum vertical amplitude ($z_{max} = 0.26$ kpc), very low inclination and the shape of its meridional orbit (Fig. 6). But due to its high eccentricity ($e=0.74$) and retrograde velocity ($V = -54$ km s^{-1}), it clearly has a halo orbit; cf. Randall et al. (2015).

HE 1256–2738 (Pb) immediately presented as a halo orbit. It has a very low galactic rotational velocity and a very high eccentricity of 0.86. It also has a very close approach to the galactic centre with a pericentre value of 0.59 kpc, which could account for its deviation from a circular orbit.

HE 2218–2026, an intermediate-helium hot subdwarf, stands out as having a halo orbit with a large radial, low rotational velocity and a chaotic orbit (Fig. 6) that closely approaches the galactic centre. All of its orbital parameters are characteristic of the halo. At 18 kpc, it has the highest z_{max} of any of the stars in this sample. The Galactic rest-frame velocity of 321 km s^{-1} is not high enough to be classified as a hyper-velocity star, i.e. as having rest-frame velocity greater than that of the local Galactic escape velocity (≈ 500 km s^{-1}), cf. the review by Brown (2015).

UVO 0825–08 (Ca, Ge, Y, Pb), *HE 1238–1745* and HS 1051+2933 are all marginally outside the thick disc 3σ contour and have $z_{max} = 0.86$, 2.08 and 3.76 kpc, respectively. HS 1051+2933 is clearly a halo star, the other two are marginally halo/thick disc stars. We have been conservative in assigning stars to the lower energy population.

PG 0909+276 and UVO 0512–08 (Sc, Ti, V, Mn, Ni), although chemically interesting intermediate-helium subdwarfs, appear to show typically thin disc orbits.
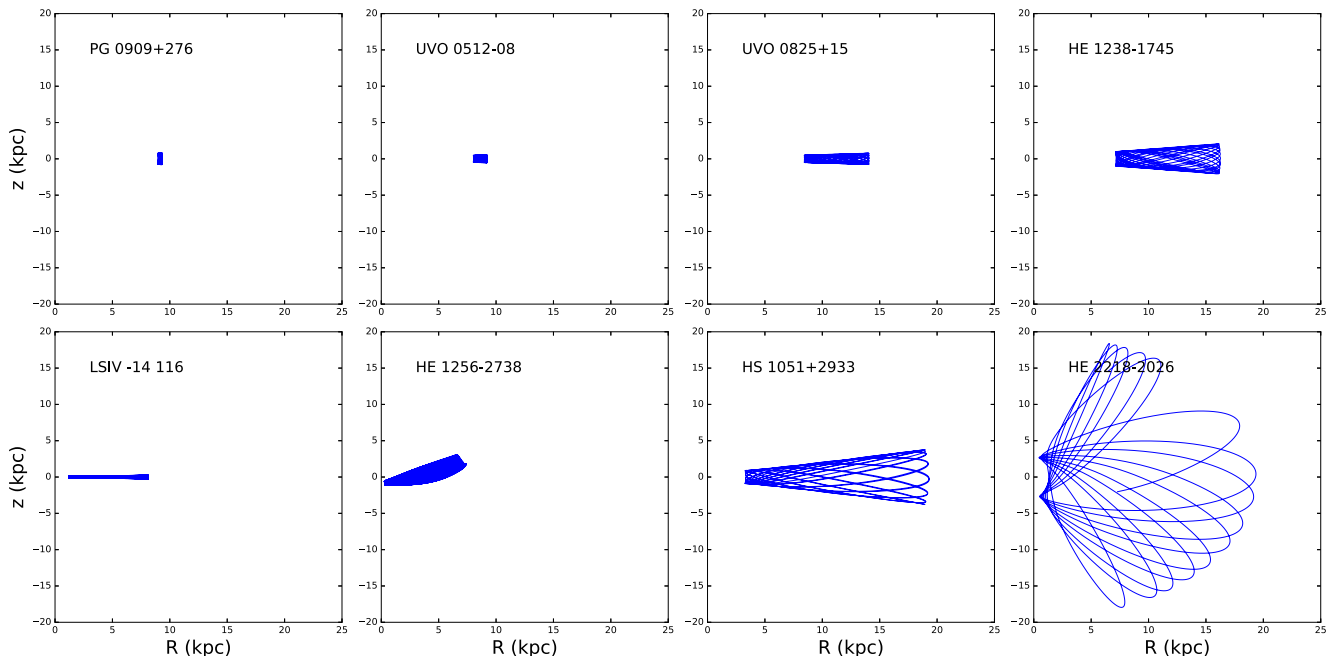

Figure 6. Meridional sections of the orbits of 8 stars. Columns 1−2 in row 1 are examples of probable thin disc stars and columns 2−4 include probable thick disc orbits. Row 2 contains probable halo orbits.
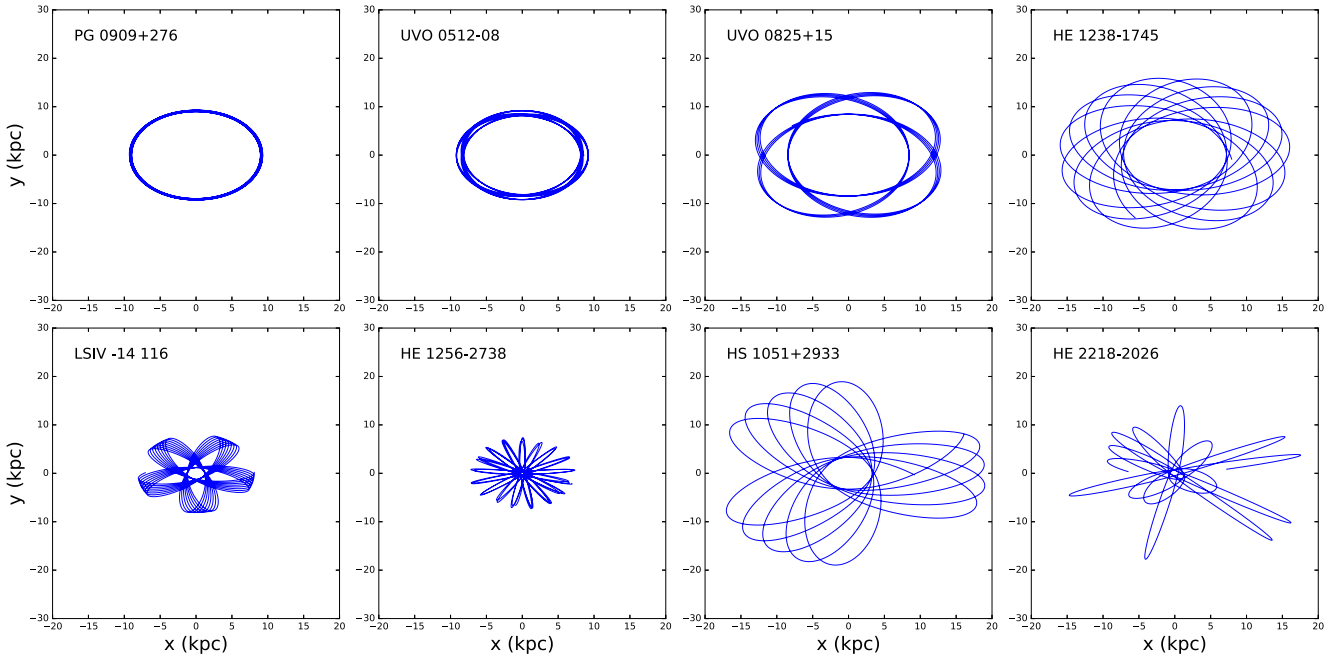
Figure 7. As Fig. 6, but projected on the *x*–*y* Galactic plane.

These results are helpful for interpreting the evolutionary origin of all types of hot subdwarfs. For the helium-deficient or ' normal' sdB stars, an origin in a close binary system is considered likely for the majority; indeed, 15/38 of the sample are confirmed binaries. Whether these systems originate in one or more common-envelope ejection episodes, or in a stable Roche lobe overflow episode, the age and mass of the progenitor are closely linked by the progenitor main-sequence lifetime. Models imply that binary sdB progenitors may have masses in the range of $0.8 < M_{MS}/M_\odot < 5$ or more (Han et al. 2002), implying possible ages anywhere between 0.2 and 10 Gyr, and hence an origin in either disc or halo. Significantly, the fractions for both classes of helium-rich subdwarfs are much lower; only one intermediate-helium subdwarf, CD–20°1123, is a confirmed close binary (Naslim et al. 2012).

For extreme-helium subdwarfs, Zhang & Jeffery (2012) argue for an origin in a merging double-helium white dwarf binary. Such systems require a significant delay between formation of the double white dwarf and the subsequent merger because, for these stars, orbital decay by gravitational radiation has a time-scale $\geq$1 Gyr. Binary star population synthesis studies show that double helium-white dwarf progenitor systems must have formed at least 2 Gyr ago, with 95 per cent formed more than 4 Gyr ago (Yu & Jeffery 2011; Zhang et al. 2014). One would therefore expect kinematics representative of an older population, as suggested by Table 5.

The intermediate-helium subdwarfs present more of a challenge. Naslim et al. (2011, 2013) have argued that the extreme surface abundances seen in LS IV$-14°$116 and the lead stars HE 2359–2844 and HE 1256–2738 are proto-subdwarfs, evolving *on to* the extended horizontal branch. Their atmospheres should consequently represent a snapshot of an evolving surface chemistry in which radiative levitation and gravitational settling continually resort the surface layers as the star evolves and helium sinks out of the photosphere. For this to be true, the intermediate-helium subdwarfs should share the kinematical properties of the helium-deficient subdwarfs. If the fraction of halo stars in each subsample (Table 5) is representative of age, then the intermediate-helium subdwarfs (4 halo/27 stars)

would appear to be older than both the helium-deficient (1/38) and the extreme-helium subdwarfs (2/23). However, the statistics are at best small. Radial velocities have not been obtained in a uniform manner so that a high fraction of extreme-helium subdwarfs have only single epoch data, whilst the other groups are represented by multi-epoch data. Similarly, the sample space volumes are slightly different, with mean distances for the three groups being $\langle d \rangle = 1.13 \pm 0.89$ kpc (intermediate), $\langle d \rangle = 1.39 \pm 0.90$ kpc (extreme) and $\langle d \rangle = 1.07 \pm 0.79$ kpc (helium-deficient). This could account for the slightly lower energy classification of the helium-deficient group with respect to the helium-rich groups. Moreover, our sample of helium-deficient subdwarfs omits a more distant sample of halo sdBs. Tillich et al. (2011) identified two distinct kinematic groups: normal halo subdwarfs with low Galactic rotation and extreme halo subdwarfs on highly eccentric retrograde orbits. The presence of two distinct groups indicates different origins. The normal halo sdBs might have been ejected into the halo via the slingshot mechanism. The extreme halo stars might originate in the outskirts of the Galactic disc and not in the central bulge. It is therefore not unreasonable to suspect that the intermediate-helium subdwarfs equally show such a diverse range of kinematical properties.

However, it is puzzling that the two intermediate-helium subdwarfs with the most extreme chemistries are in halo orbits. An intriguing alternative is that these stars represent the ejecta from Type Ia supernovae, as suggested for the hyper-velocity compact helium star US 708 (Justham et al. 2009; Geier et al. 2013). A hot subdwarf having a massive white dwarf companion in a short-period orbit, such as CD$-30°$11223, will, towards the end of core helium burning, expand and transfer mass to its companion, potentially stripping the hydrogen layers from the subdwarf and leading to a thermonuclear explosion in the white dwarf. The explosion will have the consequences of (i) contaminating the helium-rich subdwarf remnant with heavy-metal ejecta from the supernova and (ii) unbinding it with a velocity close to the orbital velocity at the time of explosion $\approx$300–500 km s^{-1} (Liu et al. 2013). The result is a chemically peculiar helium-rich subdwarf in a

halo-like orbit. Whether bound or unbound will depend on the sub-dwarf velocity vector relative to the Galactic potential at the time of explosion.

6 CONCLUSION

The space motions and Galactic orbits of 88 hot subdwarfs were computed from published proper motions, radial velocities and inferred distances. The orbital parameters were used to classify sample members as having disc or halo orbits. This study confirms that sdO/B stars are members of all Galactic populations. The sample was divided into helium-deficient (or *normal*), intermediate-helium and extreme-helium subdwarfs based on their surface helium abundances, in order to establish whether the different groups could be distinguished kinematically. Of the samples studied, helium-deficient sdO/Bs show the lowest standard deviations in all orbital parameters discussed here and are likely to be primarily disc stars. However, at least one and possibly two populations of halo sdB stars are also known to exist (Tillich et al. 2011). Both samples of He-rich subdwarfs appear to have similar kinematics, primarily comprising disc stars with a small fraction of halo objects.

Three intermediate-helium stars, including two with peculiar surface chemistries, show quite extreme halo orbits, but their space velocities are insufficient for them to be *bona fide* hyper-velocity stars. The high velocities argue *against* a previously proposed connection between the chemically peculiar and normal hot subdwarfs but pose equally challenging questions concerning the origin of the former. The possibility that they are the polluted ejecta from Type Ia supernovae appears to be worth exploring further.

The primary limitation of this study is the small sample size, particularly with regard to the extreme- and intermediate-helium subsamples. In the near future, the *Gaia* spacecraft will deliver distances and proper motions having two orders of magnitude better precision than currently available; many of the questions raised here will be addressed within a very few years.

ACKNOWLEDGEMENTS

REFERENCES

Adelman-McCarthy J. K. et al., 2008, VizieR Online Data Catalog, 2282, 0
Ahmad A., Jeffery C. S., 2003, A&A, 402, 335
Ahmad A., Behara N. T., Jeffery C. S., Sahin T., Woolf V. M., 2007, A&A, 465, 541

---

[1] http://www.cosmos.esa.int/gaia
[2] http://www.cosmos.esa.int/web/gaia/dpac/consortium

Altmann M., Edelmann H., de Boer K. S., 2004, A&A, 414, 181
Arenou F. et al., 2017, A&A, preprint (arXiv:1701.00292)
Astraatmadja T. L., Bailer-Jones C. A. L., 2016, preprint (arXiv:e-print)
Aznar Cuadrado R., Jeffery C. S., 2002, A&A, 385, 131
Beers T. C., Doinidis S. P., Griffin K. E., Preston G. W., Shectman S. A., 1992, AJ, 103, 267
Beers T. C., Rossi S., O'Donoghue D., Kilkenny D., Stobie R. S., Koen C., Wilhelm R., 2001, VizieR Online Data Catalog, 732, 451
Bobylev V. V., Goncharov G. A., Bajkova A. T., 2007, VizieR Online Data Catalog, 908, 30821
Bovy J., 2011, PhD thesis, New York University
Bovy J., 2015, ApJ, 216, 29
Brown W. R., 2015, ARA&A, 53, 15
Brown W. R., Beers T. C., Wilhelm R., Allende Prieto C., Geller M. J., Kenyon S. J., Kurtz M. J., 2008, AJ, 135, 564
Colin J. et al., 1994, A&A, 287, 38
Copperwheat C. M., Morales-Rueda L., Marsh T. R., Maxted P. F. L., Heber U., 2011, MNRAS, 415, 1381
Downes R. A., 1986, ApJS, 61, 569
Drilling J. S., Moehler S., Jeffery C. S., Heber U., Napiwotzki R., 2003, in Gray R. O., Corbally C. J., Philip A. G. D., eds, The Garrison Festschrift. L. Davis Press, Schenectady, p. 27
Drilling J. S., Jeffery C. S., Heber U., Moehler S., Napiwotzki R., 2013, A&A, 551, A31
Edelmann H., 2003, PhD thesis, Friedrich-Alexander University
Gaia Collaboration, 2016a, A&A, 595, A1
Gaia Collaboration, 2016b, A&A, 595, A2
Geier S. et al., 2013, A&A, 554, A54
Geier S. et al., 2015, A&A, 577, A26
Gontcharov G. A., 2006, Astron. Astrophys. Trans., 25, 145
Han Z., Podsiadlowski P., Maxted P. F. L., Marsh T. R., Ivanova N., 2002, MNRAS, 336, 449
Han Z., Podsiadlowski P., Maxted P. F. L., Marsh T. R., 2003, MNRAS, 341, 669
Heber U., 1986, A&A, 155, 33
Heber U., 2009, ARA&A, 47, 211
Heber U., 2016, PASP, 128, 082001
Heber U., Dreizler S., Werner K., Engels D., Hagen H.-J., 1996, in Jeffery C. S., Heber U., eds, ASP Conf. Ser. Vol. 96, Hydrogen Deficient Stars. Astron. Soc. Pac., San Francisco, p. 241
Irrgang A., Wilcox B., Tucker E., Schiefelbein L., 2013, A&A, 549, A137
Jeffery C. S. et al., 2017, MNRAS, 465, 3101
Justham S., Wolf C., Podsiadlowski P., Han Z., 2009, A&A, 493, 1081
Karl C., Heber U., Jeffery S., Napiwotzki R., Geier S., 2006, Balt. Astron., 15, 151
Kawka A., Vennes S., O'Toole S., Németh P., Burton D., Kotze E., Buckley D. A. H., 2015, MNRAS, 450, 3514
Kharchenko N. V., Scholz R.-D., Piskunov A. E., Röser S., Schilbach E., 2007, Astron. Nachr., 328, 889
Kilkenny D., Muller S., 1989, South Afr. Astron. Obs. Circ., 13, 69
Kordopatis G. et al., 2013, VizieR Online Data Catalog, 355, 50012
Lindegren L. et al., 2016, A&A, 595, A4
Liu Z.-W. et al., 2013, ApJ, 774, 37
Luo A.-L. et al., 2015, Res. Astron. Astrophys., 15, 1095
Ma X., Hopkins P. F., Wetzel A. R., Kirby E. N., Angles-Alcazar D., Faucher-Giguere C.-A., Keres D., Quataert E., 2016, preprint (arXiv:e-prints)
Maxted P. f. L., Heber U., Marsh T. R., North R. C., 2001, MNRAS, 326, 1391
Miyamoto M., Nagai R., 1975, PASJ, 27, 533
Moehler S., Richtler T., de Boer K. S., Dettmar R. J., Heber U., 1990, A&A, 86, 53
Napiwotzki R. et al., 2003, in de Martino D., Silvotti R., Solheim J.-E., Kalytis R., eds, NATO ASIB Proc. 105: White Dwarfs. Kluwer, Dordrecht, p. 39
Naslim N., Jeffery C. S., Ahmad A., Behara N. T., Şahìn T., 2010, MNRAS, 409, 582
Naslim N., Jeffery C. S., Behara N. T., Hibbert A., 2011, MNRAS, 412, 363

Naslim N., Geier S., Jeffery C. S., Behara N. T., Woolf V. M., Classen L., 2012, MNRAS, 423, 3031

Naslim N., Jeffery C. S., Hibbert A., Behara N. T., 2013, MNRAS, 434, 1920

Navarro J. F., Frenk C. S., White S. D. M., 1996, ApJ, 462, 563

O'Toole S. J., Heber U., 2006, A&A, 452, 579

Pauli E.-M., Napiwotzki R., Altmann M., Heber U., Odenkirchen M., Kerber F., 2003, A&A, 400, 877

Pauli E.-M., Napiwotzki R., Heber U., Altmann M., Odenkirchen M., 2006, A&A, 447, 173

Randall S. K., Bagnulo S., Ziegerer E., Geier S., Fontaine G., 2015, A&A, 576, A65

Roeser S., Demleitner M., Schilbach E., 2010, AJ, 139, 2440

Schlafly E. F., Finkbeiner D. P., 2011, ApJ, 737, 103

Sperauskas J., Bartkevicius A., 2002, Astron. Nachr., 323, 139

Stroeer A., Heber U., Lisker T., Napiwotzki R., Dreizler S., Christlieb N., Reimers D., 2007, A&A, 462, 269

Tillich A. et al., 2011, A&A, 527, A137

van Leeuwen F., 2007, A&A, 474, 653

Yu S., Jeffery C. S., 2011, MNRAS, 417, 1392

Zacharias N., Monet D. G., Levine S. E., Urban S. E., Gaume R., Wycoff G. L., 2004, Am. Astron. Soc. Meeting Abstr., 36, 1418

Zhang X., Jeffery C. S., 2012, MNRAS, 419, 452

Zhang X., Jeffery C. S., Chen X., Han Z., 2014, MNRAS, 445, 660

Ziegerer E., Volkert M., Heber U., Irrgang A., Gänsicke B. T., Geier S., 2015, A&A, 576, L14

APPENDIX A

The input data, including radial velocities, proper motions and inferred distances for each of the three subdwarf groups are presented in Tables A1–A3. The orbital parameters, space motions and inferred population are presented in Tables A4–A6. The table contents are described fully in the text (Sections 2 and 3).

Table A1. Input data for the intermediate helium-rich stars. [†]Highlights confirmed binary systems in which case the system velocity γ is quoted. [*]Corresponds to single epoch radial velocity measurements. [‡]marks distances obtained from Astraatmadja & Bailer-Jones (2016).

Star	RV km s^{-1}	±	ref	μ_α mas yr^{-1}	±	μ_δ mas yr^{-1}	±	ref	M_B	d kpc	±
UVO 0512–08	11.0	3.3	a	−28.5	1.3	−24.0	2.9	PPMXL	...	0.22	0.03
BPS CS 22946–0005	−57	10	b	3.2	4.1	−3.5	4.1	PPMXL	...	1.30	0.21
BPS CS 22956–0094	−21	10	b, t	37.3	2.8	−27.5	2.8	NOMAD	...	0.59	0.09
CPD–20°1123[†]	−6.3	1.2	c	6.6	1.7	−14.8	3.6	NOMAD	...	0.29	0.05
HD 127493	7	3	de	−32.9	1.3	−16.6	1.2	PPMXL	...	0.11	0.02
HE 1135–1134	24.67	2.45	t	−9.4	6.0	2.3	6.0	PPMXL	3.88f	2.15	0.30
HE 1136-2504	59.39	9.22	t	−5.1	3.0	−6.6	2.8	NOMAD	4.25f	0.89	0.12
HE 1238-1745	-7.87	2.72	t	12.4	5.0	3.1	5.0	PPMXL	3.83f	1.33	0.18
HE 1256-2738	140.46	5.6	t	−11.3	6.6	−10.6	6.6	PPMXL	4.04f	3.16	0.49
HE 1310–2733	41.54	1.82	t	−6.5	4.6	0.6	4.6	NOMAD	3.76f	1.39	0.19
HE 2218–2026	−278.86	1.45	t	20	4	−4	1	NOMAD	4.40f	2.50	0.35
HE 2357–3940	−18.38	14.15	g	15.8	1.2	3.7	1.2	NOMAD	...	0.15	0.02
HE 2359-2844	−90.71	3.03	t	2	3	−12	3	NOMAD	3.85f	2.42	0.33
HS 1051+2933	−130	3	h	14	3	−16	3	NOMAD	4.70h	1.96	0.27
JL 87	−6.1	2.3	i	−0.4	1.06	3.77	1.49	*GAIA*	...	0.58	0.14[‡]
LS IV−14°116	−150	2	j	9.2	1.8	−130.6	1.8	PPMXL	...	0.44	0.20
PG 0229+064	7.6	4.0	k	−16.0	1.9	−2.0	1.9	PPMXL	...	0.33	0.05
PG 0240+046	63.4	2.0	k	28.4	2.7	−5.4	2.6	PPMXL	...	0.77	0.12
PG 0909+276	20.0	2	h	0.5	1.0	0.1	0.9	NOMAD	...	0.87	0.14
SB 705	4	12	a	10.36	0.53	9.84	0.61	*GAIA*	...	0.67	0.16[‡]
TON 107	28.5	2.8	l	−2	6	−14	5	NOMAD	...	2.08	0.34
UVO 0825+15	56.4*	0.5	t	−23.7	1.2	−0.2	1.2	NOMAD	...	0.33	0.05
SDSS J092440.11+305013.16	2.7*	0.5	t	0.2	4.5	−10.4	4.5	PPMXL	...	1.01	0.16
SDSS J160131.30+044027.00	-26.7*	0.9	t	−14.8	4.3	0.2	4.3	PPMXL	...	0.89	0.14
SDSS J175137.44+371952.37	-73.6*	0.2	t	−9.3	4.2	0.5	4.2	PPMXL	...	1.32	0.21
SDSS J175548.50+501210.77	-62.7*	0.2	t	−9.9	1.6	25.2	1.6	PPMXL	...	0.42	0.07
HS 1000+471	0*	10	t	−1.5	5.6	−5.8	5.6	PPMXL	...	4.14	0.65

References. a. Kilkenny & Muller (1989), b. Beers et al. (1992), c. Naslim et al. (2012), d. Bobylev, Goncharov & Bajkova (2007), e. Kharchenko et al. (2007), f. Stroeer et al. (2007), g. Kordopatis et al. (2013), h. Edelmann (2003), i. Ahmad et al. (2007), j. Randall et al. (2015), k. Aznar Cuadrado & Jeffery (2002), l. Luo et al. (2015), t. This paper: Table 1

Table A2. Input data for the extreme helium-rich stars. Symbols as in Table A1.

Star	RV km s^{-1}	±	ref	μ_α mas yr^{-1}	±	μ_δ mas yr^{-1}	±	ref	M_B	d kpc	±
BPS CS 22940–0009	37	10	*a, t*	2.8	5.2	− 14.4	5.2	NOMAD	...	0.77	0.12
BPS CS 29496–0010	− 39.8	0.1	*t*	− 19.0	4.3	− 1.2	4.3	PPMXL	...	1.11	0.17
HE 0001–2443	3.98	0.71	*t*	6	2	− 26	3	NOMAD	4.62*i*	0.66	0.1
HE 0342-1702	− 15*	10	*a*	− 3.0	5.6	− 8.8	5.6	PPMXL	...	0.73	0.10
HE 1251+0159	3*	24	*b*	8	2	− 18	3	NOMAD	4.47*i*	1.55	0.22
LB 3229	24	28	*c, t*	16.2	5.2	− 4.4	5.3	NOMAD	...	0.66	0.10
PG 0039+135	− 92*	66	*d*	− 2.6	4.9	1.8	5.4	NOMAD	...	0.33	0.05
PG 1413+114	23.2	17	*e*	− 1.4	4.6	− 16.8	4.6	PPMXL	...	1.99	0.31
PG 1536+690	− 295	15	*f*	0	2	− 20	4	NOMAD	...	0.96	0.15
PG 2321+214	− 19.7*	3	*t*	23.9	4.6	− 8.9	4.9	NOMAD	...	0.49	0.08
PG 2352+181	− 49*	38	*d*	26.3	4.9	− 3.4	5.2	NOMAD	...	0.38	0.06
PG 0902+057	− 15*	5	*t*	− 15.4	4.4	− 6.3	4.4	PPMXL	...	0.93	0.15
PG 1615+413	− 80*	5	*t*	− 6.9	5.6	− 13.5	5.6	PPMXL	...	2.88	0.45
PG 1600+171	− 78*	5	*t*	− 10.5	5.2	− 4.9	5.2	PPMXL	...	3.14	0.47
PG 1658+273	− 33*	5	*t*	− 19.2	4.4	− 0.7	4.4	PPMXL	...	2.33	0.37
PG 1715+273	31*	5	*t*	− 2.0	3	− 6.0	1	NOMAD	...	2.91	0.46
HS 1844+637	20*	10	*t*	− 5.0	5.6	1.3	5.6	PPMXL	...	2.7	0.42
PG 1554+408	73*	8	*t*	− 5.1	5.4	− 3.3	5.4	PPMXL	...	2.34	0.37
PG 2258+155	34*	5	*t*	0.6	5.3	− 5.6	5.3	PPMXL	...	1.65	0.26
PG 1127+019	19*	2	*t*	− 7.1	4.1	− 9.2	4.1	PPMXL	...	0.62	0.01
PG 1415+492	54*	1	*t*	− 1.3	4	− 3.8	4	PPMXL	...	1.17	0.18
PG 2215+151	− 13*	5	*t*	3.1	5.5	15.1	5.1	NOMAD	...	0.96	0.15
PG 1544+488[†]	− 25.5	0.4	*t*	− 44	3	34	1	NOMAD	...	0.55	0.09

References. *a*. Beers et al. (1992), *t*. This paper: Table 1, *b*. Adelman-McCarthy et al. (2008), *c*. Kilkenny & Muller (1989), *d*. Brown et al. (2008), *e*. Geier et al. (2015), *f*. Heber et al. (1996), *i*. Stroeer et al. (2007)

Table A3. Input data for the helium-deficient stars. Symbols as in Tables A1 and A2.

Star	RV km s^{-1}	±	ref	μ_α mas yr^{-1}	±	μ_δ mas yr^{-1}	±	ref	M_B	d kpc	±
CD –35°15910	25.7*	2.8	a	− 21.4	1.8	− 6.2	1.5	PPMXL	...	0.22	0.06
Feige 65	53.5*	2	c	4.1	1.3	− 11.9	1.3	PPMXL	...	0.35	0.09
HD 205805	−71.0*	4	c	76.7	1.1	− 10.2	0.8	PPMXL	...	0.15	0.04
HD 4539	−4*	2	c	5.09	1.50	25.19	1.00	PPMXL	...	0.15	0.04
HE 0004–2737	31.56§	28.91	b	17.5	3.0	− 11.5	2.8	NOMAD	4.8c	0.62	0.09
HE 0151–3919	−48*	15	e	− 9.2	9.4	− 41.4	9.4	PPMXL	...	1.07	0.27
HE 0407–1956	59*	30	d	8.5	4.1	2.1	4.1	PPMXL	3.8c	0.86	0.12
HE 1318–2111†	48.9	0.7	f	2.7	12.3	− 1.1	12.3	NOMAD	3.3c	2.04	0.28
HE 2135–3749†	45.0	0.5	i	17.1	9.8	− 1.2	9.8	PPMXL	4.7c	0.66	0.10
HE 2337–2944	7	10	d	19.9	4.3	− 7.3	4.3	PPMXL	4.5c	0.90	0.13
HS 0232+3155	−11*	30	c	2.8	4.3	− 1.9	4.3	PPMXL	4.1c	1.95	0.27
HS 0233+3037	−129 *	30	c	8.2	4.3	− 11.4	4.3	PPMXL	4.3c	1.23	0.17
HS 0546+8009	7*	30	c	6.5	4.1	1.2	4.1	PPMXL	4.1c	1.10	0.15
HS 0815+4243	41*	30	c	4.2	5.4	− 5.2	5.4	PPMXL	4.6c	2.60	0.35
HS 1236+4754	−46.6	1.1	g	− 14	1	2	6	NOMAD	4.1c	1.99	0.27
HS 1320+2622	−110 *	30	c	− 8.7	4.7	− 1.2	4.7	PPMXL	4.1c	3.14	0.43
HS 1739+5244	−28*	30	c	− 2	2	− 6	1	NOMAD	3.5c	1.76	0.24
HS 1741+2133	−84*	30	c	− 13.2	5.1	− 5.2	5.1	PPMXL	3.1c	1.95	0.27
HS 2156+2215	−22*	30	c	− 2.5	4.6	− 2.3	4.6	NOMAD	3.0c	3.05	0.42
HS 2201+2610	−31*	30	c	− 0.7	4.1	− 6.1	4.1	PPMXL	4.0c	0.95	0.13
HS 2208+2718	124*	30	c	4.3	4.8	− 7.2	4.8	PPMXL	3.9c	1.28	0.18
HS 2242+3206	−168*	30	c	28.2	3.3	6.9	3.3	PPMXL	4.3c	1.48	0.20
KPD 0054+5406	−35.5	5.0	h	− 2.0	0.4	− 0.4	0.4	PPMXL	...	0.57	0.14
KPD 2040+3955†	−16.4	1.0	b	− 8.9	5.6	− 10.2	5.6	NOMAD	...	1.03	0.26
KPD 2215+5037†	−7.2	1.0	b	16	12	18	4	NOMAD	...	0.48	0.12
KUV 16256+4034†	−90.9	0.9	f	− 19.3	0.8	− 13.2	0.6	NOMAD	...	0.48	0.12
PG 0004+133	−1.88	3.9	b	− 0.5	5.0	− 20.7	5.2	NOMAD	...	0.47	0.12
PG 0005+179	−15.99§	32.94	b	19.2	5.0	− 2.0	5.3	NOMAD	...	0.83	0.21
PG 0919+273†	−68.6	0.6	b	23.1	0.7	− 25.5	1.2	NOMAD	...	0.44	0.11
PG 0934+186†	7.7	3.2	b	− 20.7	4.4	− 6.2	4.7	NOMAD	...	0.55	0.14
PG 1136-003†	63	14	f	− 6.4	5.5	− 20.7	5.5	NOMAD	...	0.87	0.23
PG 1230+052†	43.1	0.7	b	− 3.2	5.8	− 20.2	6.4	NOMAD	...	0.69	0.17
PG 1244+113†	7.4	0.8	b	0.0	4.9	− 8.5	5.3	NOMAD	...	0.34	0.09
PG 1403+316†	−2.1	0.9	b	− 34.3	2.1	4.5	2.1	NOMAD	...	0.98	0.25
PG 1519+640†	0.9	0.8	b	28.1	2.3	41.2	2.5	NOMAD	...	0.39	0.10
PG 1558-007†	−71.9	0.7	b	− 4.4	5.6	− 7.9	5.5	NOMAD	...	0.99	0.25
PG 1648+536†	−69.9	0.9	f	− 3.8	4.2	0.1	4.2	PPMXL	...	1.19	0.30
PG 2331+038†	−9.5	1.1	b	− 9.2	4.6	6.5	4.7	PPMXL	...	0.84	0.21
PHL 932	18	2	c	36.1	2.9	7	2	NOMAD	...	0.35	0.09

References. *a*. Gontcharov (2006), *b*. Copperwheat et al. (2011), *c*. Edelmann (2003), *d*. Beers et al. (1992), *e*. Beers et al. (2001), *f*. Geier et al. (2015), *g*. Sperauskas & Bartkevicius (2002), *h*. Downes (1986), *i*. Karl et al. (2006) § These stars show signs of orbital variation; the data are insufficient to extract γ. Here, the mean radial velocities and standard deviations are used.

Table A4. Orbital parameters, galactic velocities and 1σ errors for the intermediate helium-rich stars. The last column shows the Galactic population in which each star has been classified. TH = thin disc, TK = thick disc and H = halo.

Star	R_a kpc	±	R_p kpc	±	z_{max} kpc	±	e	±	J_z kpc km s⁻¹	±	z_n	±	U km s⁻¹	±	V km s⁻¹	±	W km s⁻¹	±	pop
UVO 0512−08	9.22	0.20	8.03	0.12	0.54	0.12	0.07	0.01	2059.50	23.50	0.07	0.01	−23.9	3.82	248.53	18.42	−31.29	3.36	TH
BPS CS 22946−0005	8.93	0.59	7.42	1.53	2.04	0.29	0.09	0.10	1853.26	219.21	0.27	0.07	−13.06	23.90	224.38	20.36	63.67	3.61	TK
BPS CS 22956−0094	9.11	0.28	3.85	0.57	0.43	0.08	0.41	0.07	1361.16	128.91	0.05	0.01	87.27	11.08	178.99	9.73	−4.03	3.07	TK
CPD−20°1123	9.47	0.09	7.48	0.26	0.16	0.04	0.12	0.02	2024.59	31.41	0.02	0.00	−36.57	4.64	242.33	17.12	9.83	2.22	TH
HD 127493	8.36	0.04	7.14	0.22	0.18	0.02	0.08	0.01	1878.41	30.77	0.02	0.00	−7.92	2.76	234.80	18.07	11.27	3.85	TH
HE 1135−1134	9.38	2.19	6.67	2.14	1.75	0.52	0.17	0.17	1820.26	376.82	0.20	0.10	43.25	47.84	226.41	27.68	12.20	9.35	TK
HE 1136−2504	8.42	0.11	4.50	0.46	0.60	0.09	0.30	0.05	1450.76	89.45	0.09	0.01	−30.86	11.37	183.83	18.69	13.59	4.94	TH
HE 1238−1745	16.25	4.18	7.18	0.46	2.08	0.75	0.39	0.12	2353.45	192.97	0.17	0.09	−99.14	32.01	301.97	17.78	19.34	7.72	TK
HE 1256−2738	7.62	0.65	0.59	0.17	3.11	0.41	0.86	0.04	−112.76	470.87	0.58	0.20	19.56	68.96	−4.39	21.24	−37.87	5.24	H
HE 1310−2733	7.84	0.20	5.30	1.14	1.14	0.37	0.19	0.10	1516.45	172.76	0.20	0.07	−19.49	25.31	204.22	23.06	37.22	3.34	TH
HE 2218−2026	19.52	4.69	1.30	0.66	18.34	5.68	0.87	0.08	194.61	201.52	1.91	2.33	303.88	39.04	38.31	13.62	96.10	13.19	H
HE 2357−3940	8.71	0.23	8.32	0.05	0.34	0.22	0.02	0.02	2049.08	14.24	0.04	0.03	4.24	3.79	253.41	20.50	22.22	8.09	TH
HE 2359−2844	8.38	0.05	1.92	1.10	4.39	0.58	0.63	0.17	604.14	328.53	1.94	5.16	−30.98	26.23	115.55	14.53	93.06	5.27	TK
HS 1051+2933	19.33	3.26	3.33	0.86	3.76	0.54	0.71	0.08	1437.27	284.00	0.20	0.05	−227.82	22.18	163.53	7.65	−55.98	2.23	H
JL 87	9.59	0.42	8.01	0.15	0.70	0.13	0.09	0.03	2084.43	35.84	0.08	0.02	28.63	10.31	257.23	20.95	3.86	6.08	TH
LS IV−14°116	8.12	0.20	1.19	2.28	0.26	0.38	0.74	0.33	−523.81	476.48	0.03	0.05	15.84	31.97	−53.99	29.73	−7.89	27.66	H
PG 0229+064	10.69	0.41	8.40	0.06	0.31	0.07	0.12	0.02	2248.48	36.62	0.04	0.01	−23.61	3.10	270.10	19.24	−7.01	3.13	TH
PG 0240+046	10.18	0.28	4.36	0.62	0.61	0.09	0.40	0.07	1524.02	134.50	0.06	0.01	88.99	16.76	181.23	12.97	−8.31	3.28	TK
PG 0909+276	9.36	0.35	9.00	0.10	0.80	0.12	0.02	0.02	2172.43	40.45	0.09	0.01	−4.36	6.63	249.77	17.57	22.41	2.30	TH
SB 705	10.52	0.98	7.87	0.26	0.39	0.07	0.14	0.06	2161.18	41.51	0.05	0.05	−22.65	5.64	265.48	19.55	6.53	2.34	TH
TON 107	9.28	0.69	3.54	1.92	3.32	1.86	0.45	0.21	1125.47	481.73	0.36	0.20	−47.73	40.41	139.93	11.34	72.51	2.43	TK
UVO 0825+15	14.93	0.58	8.44	0.01	0.86	0.06	0.28	0.02	2543.88	35.38	0.09	0.01	−19.81	2.30	307.23	19.44	−31.7	2.46	TK
SDSS J092440.11 +305013.16	9.22	0.19	6.11	1.27	0.75	0.12	0.20	0.10	1783.13	199.25	0.09	0.02	−20.87	17.95	205.01	17.50	4.70	2.31	TH
SDSS J160131.30 +044027.00	8.10	0.26	5.21	0.81	0.81	0.21	0.22	0.07	1546.31	154.44	0.10	0.03	38.65	12.31	208.68	24.01	30.77	2.90	TH
SDSS J175137.44 +371952.37	8.18	0.27	3.56	0.47	0.76	0.32	0.39	0.05	1229.67	127.13	0.10	0.04	43.05	17.60	163.55	25.19	23.15	4.71	TK
SDSS J175548.50 +501210.77	8.91	0.18	4.83	0.17	0.24	0.03	0.30	0.02	1561.31	28.15	0.03	0.00	58.29	3.29	196.40	22.87	−0.59	3.23	TH
HS 1000+471	15.24	9.04	10.75	2.11	5.01	6.46	0.17	0.20	2672.06	956.10	0.37	0.58	13.11	85.32	138.81	12.14	7.36	11.62	TK

Table A5. Orbital parameters and galactic velocities for the extreme helium-rich stars.

Star	R_a kpc	±	R_p kpc	±	z_{max} kpc	±	e	±	J_z kpc km s⁻¹	±	z_n	±	U km s⁻¹	±	V km s⁻¹	±	W km s⁻¹	±	pop
BPS CS 22940−0009	7.90	0.15	4.68	0.85	0.53	0.19	0.26	0.08	1452.08	160.86	0.08	0.03	−21.95	17.29	194.19	16.63	−17.91	4.52	TH
BPS CS 29496−0010	14.87	3.14	7.17	0.46	3.03	1.01	0.35	0.09	2233.39	184.77	0.21	0.09	−84.03	12.11	282.43	26.78	75.28	2.78	H
HE 0001−2443	8.46	0.06	4.16	0.58	0.65	0.10	0.34	0.06	1383.07	125.65	0.10	0.02	−22.14	4.40	210.48	14.34	−1.11	3.63	TH
HE 0342−1702	10.26	0.93	7.48	0.85	0.59	0.10	0.16	0.05	2077.65	165.70	0.08	0.01	−50.94	16.11	243.34	21.08	4.94	4.29	TH
HE 1251+0159	11.10	0.92	3.72	0.72	2.09	0.62	0.50	0.09	1350.89	197.91	0.22	0.09	−137.71	15.89	175.63	17.17	−46.38	11.58	TK
LB 3229	8.38	0.07	5.51	0.99	0.57	0.10	0.21	0.09	1630.99	168.18	0.07	0.01	9.08	18.79	204.59	23.30	1.14	12.97	TH
PG 0039+135	8.97	0.24	6.10	1.36	1.89	0.95	0.19	0.12	1687.63	321.38	0.29	0.15	−37.5	9.78	206.38	35.29	78.71	29.10	TK
PG 1413+114	8.80	0.90	2.33	1.17	2.03	0.36	0.58	0.16	873.22	368.26	0.26	0.07	−103.25	31.16	125.49	16.15	−12.69	7.93	TK
PG 1536+690	11.54	0.71	0.99	1.04	9.76	1.48	0.84	0.15	222.93	108.13	1.29	1.05	−141.57	13.37	33.63	25.86	−148	4.64	H
PG 2321+214	8.74	0.19	5.59	0.46	0.35	0.14	0.22	0.04	1680.81	75.47	0.04	0.02	34.74	12.73	207.73	14.91	−14.52	4.34	TH
PG 2352+181	8.59	0.15	5.10	1.22	0.49	0.42	0.26	0.11	1579.87	236.22	0.06	0.05	25.36	12.19	195.09	24.67	25.45	14.90	TH
PG 0902+057	9.25	0.99	8.96	0.41	1.61	0.60	0.02	0.04	2103.74	147.58	0.18	0.07	−3.01	12.49	243.27	22.74	−62.28	2.23	TK
PG1615+413	9.03	1.61	1.69	1.57	3.18	0.53	0.68	0.27	633.66	445.89	0.44	0.16	−100.82	47.61	87.85	19.11	18.77	4.74	TK
PG1600+171	7.25	0.81	1.36	1.15	2.39	0.51	0.68	0.23	386.13	484.78	0.36	0.10	61.00	51.03	68.97	27.47	32.72	8.36	TK
PG1658+273	8.35	1.02	2.63	0.33	5.76	2.44	0.52	0.03	632.82	310.84	1.24	3.28	60.61	28.90	95.49	34.81	150.84	4.03	TK
PG1715+273	7.66	0.57	6.30	0.85	1.78	0.33	0.10	0.05	1593.18	185.26	0.27	0.06	−34.72	22.37	227.38	5.85	30.17	7.88	TK
HS1844+637	11.36	1.70	7.40	2.29	2.61	2.36	0.21	0.20	2037.64	342.34	0.25	0.25	60.76	59.10	236.59	25.46	74.93	10.65	TK
PG1554+408	10.03	2.88	7.89	0.90	3.77	0.81	0.12	0.16	1867.92	380.46	0.47	0.25	3.93	49.11	243.61	22.08	101.52	6.73	TK
PG2258+155	9.76	1.77	8.40	0.60	1.62	0.47	0.07	0.09	2094.75	228.02	0.17	0.05	7.70	35.24	256.79	17.59	−44.41	6.27	TK
PG1127+019	8.51	0.08	6.22	0.60	0.56	0.03	0.15	0.05	1751.48	87.32	0.07	0.01	−12.56	10.43	215.77	18.88	5.11	2.29	TH
PG1415+492	10.56	1.65	8.48	0.06	2.24	0.20	0.11	0.08	2142.10	167.49	0.21	0.04	−3.01	20.76	261.89	18.19	64.48	4.48	TK
PG2215+151	12.30	2.04	7.51	0.50	1.58	0.79	0.24	0.09	2192.41	117.95	0.13	0.07	−233.78	12.14	215.86	20.93	31.20	16.51	TK
PG1544+488	11.23	0.80	4.34	0.45	1.05	0.32	0.44	0.07	1554.39	81.96	0.09	0.03	33.56	14.72	259.72	20.51	−24.84	6.21	TK

Table A6. Orbital parameters and galactic velocities for the helium-deficient stars.

Star	R_a kpc	±	R_p kpc	±	z_{max} kpc	±	e	±	J_z kpc km s^{-1}	±	z_n	±	U km s^{-1}	±	V km s^{-1}	±	W km s^{-1}	±	pop
CD −35°15910	9.87	0.26	7.66	0.13	0.29	0.05	0.13	0.02	2080.52	13.91	0.04	0.01	−32.24	2.57	265.86	18.34	−16.22	4.28	TH
Feige 65	9.40	0.20	8.37	0.06	1.50	0.12	0.06	0.01	2061.68	29.80	0.17	0.01	−14.71	5.48	252.57	15.06	64.24	3.82	TH
HD 205805	10.75	0.25	6.64	0.32	0.44	0.18	0.24	0.03	1994.73	31.93	0.05	0.02	76.20	5.68	243.01	14.31	24.66	2.13	TH
HD 4539	9.51	0.30	8.45	0.01	0.33	0.07	0.06	0.02	2145.20	27.70	0.04	0.01	0.85	4.73	262.19	19.06	21.12	2.22	TH
HE 0004−2737	8.40	0.08	5.54	0.64	0.88	0.37	0.20	0.06	1620.18	98.79	0.11	0.05	18.14	11.70	201.24	21.91	−4.7	15.62	TH
HE 0407−1956	9.29	0.44	6.40	1.13	0.61	0.20	0.18	0.09	1841.28	171.99	0.07	0.02	33.66	19.40	215.41	25.04	−8.82	12.76	TH
HE 1318−2111	9.53	5.60	5.38	2.70	2.01	1.90	0.28	0.29	1609.83	688.11	0.25	0.37	−95.15	97.41	223.22	22.12	28.68	21.34	TK
HE 2135−3749	8.46	2.28	7.95	0.29	1.36	0.59	0.03	0.13	1920.73	244.94	0.16	0.08	−0.18	30.72	248.84	16.15	−61.42	8.68	TH
HE 2337−2944	8.69	0.36	4.76	0.86	0.97	0.18	0.29	0.08	1501.14	170.00	0.12	0.02	46.28	21.90	217.37	18.81	−55.94	9.91	TH
HS 0232+3155	10.09	0.58	7.93	2.85	0.86	0.19	0.12	0.18	2112.29	379.73	0.09	0.02	18.99	37.19	221.40	25.13	7.12	9.79	TH
HS 0233+3037	10.08	0.53	2.83	0.82	0.88	0.76	0.56	0.10	1119.88	253.56	0.19	0.28	−79.21	22.73	129.70	22.24	33.28	14.04	TK
HS 0546+8009	9.46	1.78	8.93	0.90	1.02	0.61	0.03	0.09	2163.23	227.46	0.11	0.07	7.14	23.50	245.75	25.45	40.98	11.09	TK
HS 0815+4243	10.73	1.58	6.74	4.45	2.81	1.66	0.23	0.36	1858.99	704.73	0.42	1.64	7.17	58.53	184.18	20.76	63.79	6.19	TH
HS 1236+4754	11.11	2.20	4.98	1.76	3.61	1.83	0.38	0.09	1531.28	398.46	0.71	0.45	110.13	18.86	183.01	44.30	−49.97	14.57	TK
HS 1320+2622	9.61	1.99	5.12	2.98	5.83	1.91	0.31	0.26	1185.05	573.89	0.73	0.51	96.67	50.97	154.91	33.21	−84.9	5.15	TK
HS 1739+5244	8.44	0.12	6.54	1.55	0.97	0.14	0.13	0.11	1767.63	223.17	0.13	0.03	−16.44	11.67	221.73	21.14	3.42	16.42	TH
HS 1741+2133	7.42	0.36	1.91	1.31	1.55	0.81	0.59	0.23	712.46	296.68	0.63	1.67	26.96	30.78	106.93	33.56	60.31	10.77	TK
HS 2156+2215	8.58	1.18	7.26	2.71	1.37	0.57	0.08	0.21	1848.99	331.22	0.17	0.08	21.09	52.93	230.76	25.79	16.04	4.57	TH
HS 2201+2610	8.34	0.04	6.20	1.68	0.35	0.05	0.15	0.13	1743.14	237.88	0.04	0.01	−3.34	16.18	217.48	25.30	2.05	12.47	TK
HS 2208+2718	23.93	7.25	8.34	0.09	4.52	2.16	0.48	0.12	2841.56	251.09	0.19	0.11	21.62	32.43	347.42	19.72	−88.06	10.91	H
HS 2242+3206	11.50	1.37	0.53	0.69	0.93	0.22	0.91	0.11	234.00	270.30	0.08	0.02	179.27	26.30	37.35	19.43	18.52	3.32	TK
KPD 0054+5406	8.95	0.07	7.12	0.31	0.16	0.02	0.11	0.02	1930.35	44.49	0.02	0.00	−22.44	3.32	229.16	18.52	11.34	4.03	TH
KPD 2040+3955	9.07	0.77	6.64	0.51	0.15	0.41	0.15	0.08	1873.78	14.64	0.02	0.05	−44.22	18.04	233.62	20.29	11.49	3.21	TH
KPD 2215+5037	9.66	0.68	6.80	0.78	0.33	0.30	0.17	0.09	1940.89	59.13	0.04	0.03	53.44	25.75	237.36	13.11	20.98	5.95	TK
KUV 16256+4034	8.27	0.04	3.41	0.37	0.57	0.05	0.42	0.04	1207.94	89.08	0.08	0.01	9.62	9.55	155.33	19.50	−25.57	4.36	TH
PG 0004+133	8.72	0.21	6.78	0.58	0.50	0.22	0.13	0.04	1852.57	91.01	0.06	0.03	−25.13	9.38	226.44	15.36	−20.8	3.50	TH
PG 0005+179	9.36	0.73	5.23	1.28	0.59	0.17	0.28	0.11	1653.79	247.74	0.06	0.02	61.03	28.17	201.31	16.06	−0.41	3.57	TH
PG 0919+273	11.27	0.17	5.60	0.56	0.48	0.01	0.34	0.05	1844.09	99.11	0.07	0.00	−104.6	4.37	220.52	10.22	−15.73	4.92	TK
PG 0934+186	9.03	0.37	7.47	0.63	0.68	0.34	0.09	0.04	1962.96	101.55	0.08	0.04	22.27	6.46	233.42	22.38	−26.91	2.05	TH
PG 1136−003	8.60	0.21	3.16	0.98	0.80	0.37	0.46	0.12	1150.28	242.10	0.14	0.09	−52.42	14.98	231.22	17.93	−86.17	8.78	TK
PG 1230+052	8.62	0.26	4.39	1.00	0.84	0.13	0.33	0.10	1431.81	201.26	0.14	0.03	−45.5	16.48	255.43	21.55	3.96	5.58	TK
PG 1244+113	8.67	0.24	7.50	0.50	0.40	0.08	0.07	0.03	1946.10	73.24	0.05	0.01	−21.4	8.78	241.18	17.36	10.60	2.46	TH
PG 1403+316	10.42	0.93	3.49	0.87	1.58	0.30	0.50	0.12	1284.22	216.57	0.17	0.03	122.82	6.83	166.06	33.84	47.86	3.51	TK
PG 1519+640	16.20	2.95	8.32	0.05	1.84	1.01	0.32	0.08	2565.16	127.65	0.13	0.08	34.15	16.78	312.14	20.38	−52.7	8.42	TK
PG 1558−007	7.92	0.38	5.01	1.24	1.03	0.41	0.23	0.11	1483.40	229.31	0.14	0.06	39.30	18.44	204.22	19.91	−39.82	4.73	TH
PG 1648+536	8.42	0.18	4.75	0.76	0.93	0.25	0.28	0.07	1482.03	129.92	0.12	0.04	22.73	19.05	187.00	22.50	−21.23	6.37	TH
PG 2331+038	11.91	2.12	8.37	0.12	1.32	0.59	0.17	0.09	2303.87	145.96	0.14	0.07	10.68	16.74	263.73	25.22	7.22	6.23	TH
PHL 932	9.80	0.34	6.79	0.55	0.27	0.09	0.18	0.05	1952.07	62.56	0.03	0.01	55.02	14.12	236.66	18.74	5.29	9.70	TH

This paper has been typeset from a TeX/LaTeX file prepared by the author.